University of Texas Rio Grande Valley

ScholarWorks @ UTRGV

Mechanical Engineering Faculty Publications and Presentations

College of Engineering and Computer Science

12-2019

Investigation into the thermodynamics and kinetics of the binding of Cu2+ and Pb2+ to TiS2 nanoparticles synthesized using a solvothermal process

Jesus Cantu
The University of Texas Rio Grande Valley

John Valle
The University of Texas Rio Grande Valley

Kenneth Flores
The University of Texas Rio Grande Valley

Diego Gonzalez
The University of Texas Rio Grande Valley

Carolina Valdes
The University of Texas Rio Grande Valley

See next page for additional authors

Follow this and additional works at: https://scholarworks.utrgv.edu/me_fac

 Part of the Mechanical Engineering Commons

Recommended Citation

Cantu, J., Valle, J., Flores, K., Gonzalez, D., Valdes, C., Lopez, J., Padilla, V., Alcoutlabi, M., & Parsons, J. (2019). Investigation into the thermodynamics and kinetics of the binding of Cu2+ and Pb2+ to TiS2 nanoparticles synthesized using a solvothermal process. Journal of Environmental Chemical Engineering, 7(6), 103463. https://doi.org/10.1016/j.jece.2019.103463

This Article is brought to you for free and open access by the College of Engineering and Computer Science at ScholarWorks @ UTRGV. It has been accepted for inclusion in Mechanical Engineering Faculty Publications and Presentations by an authorized administrator of ScholarWorks @ UTRGV. For more information, please contact justin.white@utrgv.edu, william.flores01@utrgv.edu.

Authors

Jesus Cantu, John Valle, Kenneth Flores, Diego Gonzalez, Carolina Valdes, Jorge Lopez, Victoria Padilla, Mataz Alcoutlabi, and Jason Parsons

This article is available at ScholarWorks @ UTRGV: https://scholarworks.utrgv.edu/me_fac/7

Journal Pre-proof

Investigation into the thermodynamics and kinetics of the binding of Cu^{2+} and Pb^{2+} to TiS_2 nanoparticles synthesized using a solvothermal process.

Jesus Cantu[1], John Valle[1], Kenneth Flores[1], Diego Gonzalez[1], Carolina Valdes[1], Jorge Lopez[2], Victoria Padilla[2], Mataz Alcoutlabi[2], Jason Parsons[1]

1. Department of Chemistry University of Texas Rio Grande Valley
   One W. University Blvd Brownsville TX 78520

2. Department of Mechanical Engineering University of Texas Rio Grande Valley
   1201 W University Dr. Edinburg TX 78539

Highlights

- A TiS_2 nanomaterial was synthesized through a solvothermal process
- The binding of Cu^{2+} and Pb^{2+}ions from aqueous solution to the TiS_2 was pH dependent
- Lead bound by chemisorption copper bound by a combination of chemi/physi sorption
- Hard cations showed little to no effect on the binding of Pb^{2+} ions to TiS_2
- Hard cations affected Cu^{2+} ion binding to TiS_2

Abstract

In the present study, titanium (IV) sulfide (TiS_2) was synthesized and investigated for the removal of Cu^{2+} and Pb^{2+} ions from aqueous solutions. TiS_2 nanoparticles synthesized through a solvothermal synthesis were characterized using x-ray diffraction (XRD) and scanning electron microscopy (SEM). The average particle size for the TiS_2 material was determined to be 8.03 ± 0.98 nm from the diffraction pattern. Studies were performed to examine the effects of pH, temperature, time, and interfering ions on the binding of Cu^{2+} and Pb^{2+} to the TiS_2. As well isotherm studies were performed to determine the binding capacity of TiS_2 for both Cu^{2+} and Pb^{2+} ions. The pH profile studies showed optimal binding occurred at pH 2 for the sorption of both Cu^{2+} and Pb^{2+} to the TiS_2. The isotherm studies showed the adsorption capacities at

Journal Pre-proof

temperatures of 4, 22, and 45˚C for Cu^{2+} were 243, 222, and 153 mg/g, respectively. An opposite trend in the adsorption was observed for Pb^{2+} binding to the TiS_2. The observed binding capacities for Pb^{2+} were 32, 166, and 357 mg/g, at temperatures of 4, 22, and 45˚C, respectively. The thermodynamic parameters for binding showed a non-spontaneous process for the sorption of Cu^{2+} whereas a spontaneous binding process was observed for the sorption of Pb^{2+}. Additionally, the binding of Cu^{2+} on TiS_2 in the presence of interfering ions (Na^+, K^+, Mg^{2+}, and/or Ca^{2+}) was observed to decrease at high concentrations; however, the binding of Pb^{2+} was unaffected by the presence of the same cations.

Keywords: Copper sorption, Lead sorption, TiS_2, Isotherms, Kinetics,

Journal Pre-proof

Journal Pre-proof

Introduction:

Pollution is caused when harmful or hazardous substances are introduced into the environment. Industrialization has caused the discharge of both biodegradable and non-biodegradable pollutants into the environment. These pollutants can either be organic or inorganic compounds. Heavy metals fall under the classification of non-biodegradable pollutants, which are compounds that are not decomposed or broken down and are thus persistent in the environment. Furthermore, pollution is mobile in the environment and can enter water systems, which may directly affect potable water sources. In recent years, potable water has become a global concern for both human and environmental health. The contamination of potable water can occur through anthropogenic processes such as the synthesis and application of pesticides, petroleum refining by-products and use, fertilizers synthesis and application, as well as other industrial process. Two elements, which are non-biodegradable pollutants, copper and lead are of interest due to their high number of industrial uses and the health issues upon exposure.

Most copper and lead contamination can generally be attributed to industrial processes such as: paint manufacturing, metal smelting, battery manufacturing, oil refining processes, and mining [1-3]. Improper disposal of contaminated waste, with lead or copper, can lead to the contamination potable water sources. Interestingly, copper is both an essential trace element that is required in low concentrations for growth and development, however, copper can also be considered a toxin [4]. In high amounts, Cu^{2+} primarily leads to liver toxicity but it also causes lesions to the nervous system, diarrhea, abdominal pain, lethargy, and anorexia [1, 5-7]. Lead on the other hand, has no known biological function in the human body. Contact with lead has been shown to affect the production of heme, the nervous system, and the renal system. Lead has been shown to compete with the uptake of calcium in cells as well as calcium binding with

Journal Pre-proof

phosphokinase C, which has been shown to effect neural signaling [8]. Exposure to lead readily affects children in developmental stages, since they are in a constant state of growth [9-10].

Current remediation methods for heavy metal ions from aqueous solutions include: biosorption, adsorption, extraction, precipitation, phytoremediation, and ion exchange [11-13]. Although these methods are effective for the removal of heavy metal ions, many of these techniques are either very costly or difficult to implement. For example, ion exchange involves the use of expensive resins to exchange either toxic cations or anions with non-toxic ions [12, 14]. In addition, ion exchange techniques are not ion specific, which can increase the operational expense. Alternatively, the use of precipitating agents can be very effective at removing dissolved ions, but there is an added cost for the disposal of the sludge(s) created from the process. The generation and treatment of large amounts of sludge adds additional steps and cost to the treatment process [12]. Additionally, precipitation and flocculation technologies involve the use of chemicals, which must be removed prior to consumption thus close monitoring of the chemical levels are required. On the other hand, adsorption technologies have obtained much scientific attention for the removal of heavy metal ions from water [1-3, 5, 15-20]. In recent years, adsorption technologies have incorporated the use of nanoparticles as adsorbents, which have high surface areas, high reactivities, and high binding capacities to remove contaminants from solutions.

Several nano-adsorbents have been studied to remove heavy metal ions from water solutions. Some examples of adsorbents used in the removal of toxic heavy metals from aqueous solutions are: aluminum oxides, biochar, iron oxides, graphene oxides, iron sulfides, zinc oxides, titanium dioxides, manganese oxides, copper oxides, red mud, as well as other types of materials, [1-3,5,15-20]. Inorganic nano-adsorbents have obtained a lot of interest, recently, due to their

Journal Pre-proof

high binding capacities. For example, adsorption results reported by Mahdavi *et al.*, showed that CuO nanoparticles have capacities of 14.2 mg/g for Pb^{2+} and 54.1 mg/g for Cu^{2+}, alternatively ZnO has exhibited higher capacities for both Pb^{2+} and Cu^{2+} at 112.7 mg/g and 137.5 mg/g, respectively [18]. Similarly, Tamez *et al*., showed that Fe_3O_4 had binding capacities of 37.04 mg/g and 166.67 mg/g for Cu^{2+} and Pb^{2+} ions, respectively [6]. In the same study, Tamez *et al*, also showed that Fe_2O_3 had binding capacities of 19.61 mg/g and 47.62 mg/g for Cu^{2+} and Pb^{2+}, respectively [1]. According to Fouladgar *et al.*, γ-Al_2O_3 has a binding capacity of 51.3 mg/g for Cu^{2+} at 25˚C [21]. The anatase polymorph for titanium dioxide has exhibited a binding capacity of 83.12 mg/g (401.14 µmol/g) for the adsorption of Pb^{2+} [22]. Transition metal sulfides nanomaterials have also shown promise in the removal of toxic ions from aqueous solution [23]. Materials such as Fe_7S_8 and Pyrite based materials have been shown to be successful in the removal of arsenic from aqueous solution.

In the present study Titanium (IV) sulfide (TiS_2) was of interest due to its structural properties that give rise to the electronic and chemical behavior of TiS_2 [24]. TiS_2 nanoparticles may exhibit higher binding capacitates than metal oxides due to its layered structure, which allows the intercalation of ions between the layers, as well as its electrochemical behavior. In the present study, TiS_2 was synthesized and studied for the removal of Cu^{2+} and Pb^{2+} from aqueous solution. The material was synthesized through a solvothermal process using elemental sulfur, titanium(IV) chloride, with 1-octadecene as the solvent, and at a temperature of 300°C. The synthesized TiS_2 was characterized using x-ray diffraction, which showed the correct phase was synthesized with an average particle size of 8.03 ± 0.98 nm. Various batch studies were performed to determine the effect of pH, temperature, time, thermodynamics parameters, and

Journal Pre-proof

common hard cation interferences on the binding process. In addition, the binding capacities of lead and copper to the TiS_2 nanoparticles were determined using isotherm studies.

2.0 Methodology:

2.1 Synthesis of TiS_2 nanoparticles:

The TiS_2 nanomaterial was prepared using a method similar to that described by Prakabar *et al.* [25]. In brief, the reaction was performed by dissolving 120 mmol of elemental sulfur in 250 mL of 1-octadecene and heating to 300°C. Once the reaction reached 300°C, 20 mmol of titanium (IV) chloride ($TiCl_4$) was injected into the solution and the reaction was held at 300°C for 30 min. Subsequent to heating, the reaction mixture was cooled to room temperature naturally and filtered using vacuum filtration. The filtrate was washed using a combination of toluene, acetone, and methanol to remove the solvent and any by-products formed during the reaction.

2.2 X-Ray Diffraction Analysis:

The TiS_2 nanomaterial was characterized using X-ray powder diffraction. The diffraction patterns were collected using a Bruker D2 phaser diffractometer equipped with a Co source (k_α=1.789 Å), an iron filter, and a scintillation counter detector. The reaction product was homogenized using a mortar and pestle and was placed on a sample holder. The diffraction patterns were collected from 10° to 70° (in 2θ) with a step width of 0.05° and a 5s counting time. The diffraction patterns were fitted using the Le Bail fitting procedure in the FullProf software and crystallographic data from the literature [26-28]. The average particle size was determined using a Gaussian fitting of three independent diffraction peaks and Scherer's equation.

Journal Pre-proof

2.3 SEM

Scanning Electron Microscopy (SEM) and Energy Dispersive X-ray Analysis (EDAX) were collected using a Sigma VP Carl Zeiss. The SEM was operated with accelerating voltages between 3.0 and 5.0 kV and a working distance of 5.7 mm.

2.4 pH Batch Study:

pH profile studies were performed to investigate the effect of pH on the binding of Cu^{2+} and Pb^{2+} ions to the TiS_2 nanoparticles. The binding study was performed from pH 2 to pH 6 using 300 ppb solutions of Cu^{2+} or Pb^{2+}. The pH of the Cu^{2+} and Pb^{2+} solutions was adjusted using either dilute trace metal grade HNO_3 or dilute NaOH. 4.0 mL aliquots of the pH-adjusted solutions were transferred into reaction test tubes containing 10 mg of the TiS_2 nanomaterial. In addition, control reactions were performed, which contained the pH adjusted metal ion without the TiS_2 nanomaterial. Both the reaction and control samples were equilibrated on a nutating mixer for 1 h at room temperature. Subsequent to equilibration, the reaction and control samples were centrifuged at 3,500 RPM for 5 min, the supernatants were decanted into clean test tubes, and stored for further analysis using ICP-OES. All reaction and control samples were performed in triplicate for statistical purposes.

2.5 Binding Capacity/Thermodynamics Studies:

The capacity studies of TiS_2 nanoparticles were conducted for Cu^{2+} and Pb^{2+} using solutions with the following concentrations: 0.3, 3, 30, 100, 300, and 1000 ppm. The solutions were pH adjusted to the optimal binding pH of 2, which was previously determined from the pH

Journal Pre-proof

batch study. 4.0 mL aliquots of the reaction solutions were transferred to test tubes containing 10 mg TiS_2. As previously mentioned, control samples consisted of the metal ion solution only. Both reaction and control samples were repeated in triplicate for statistical purposes. The samples and controls were equilibrated for 1 h at 4°C, 22°C, and 45°C on a nutating mixer. Subsequent to equilibration, both the reaction and control samples were centrifuged at 3,500 RPM for 5 min, the supernatants were decanted and transferred to clean test tubes and stored for further analysis using ICP-OES.

2.6 Kinetics Study:

Kinetic studies were performed to determine the rate of the reactions for the sorption of Cu^{2+} and Pb^{2+} ion onto the TiS_2 nanomaterial. The reactions were performed using solutions consisting of either 30 ppm of Cu^{2+} or Pb^{2+} were pH adjusted to pH 2, as previously mentioned the optimum binding pH, and were reacted with 10 mg of TiS_2 at various time intervals. 4.0 mL aliquots of the solutions were transferred to reaction tubes containing 10 mg TiS_2. The control samples consisted of the metal ion reaction solution only. All reactions and control samples were performed in triplicate for statistical purposes. The reaction and control samples were equilibrated on a nutating mixer at three temperatures (4°C, 22°C, and 45°C) and at the following time intervals: 15, 30, 60, and 90 min. Subsequent to equilibration, both the reaction and control samples were centrifuged at 3,500 RPM for 5 min and the supernatants were decanted and stored for further analysis using ICP-OES.

2.7 Interference Study:

Journal Pre-proof

The removal of Cu^{2+} and Pb^{2+} ions was studied in the presence of hard cations due to the possible interference on the binding process. For the study, Na^{+}, K^{+}, Mg^{2+} and Ca^{2+} were added to 300 ppb Cu^{2+} or Pb^{2+} solutions at various concentrations. The cation concentrations used were: 0.3, 3, 30, 100, 300 and 1000 ppm. Each solution was adjusted to pH 2 and 4.0-mL aliquots were transferred to reaction tubes containing 10 mg of TiS_2. The control samples consisted of the mixed metal ion solution without the TiS_2 nanomaterial. Both the reaction and control samples were performed in triplicate for statistical purposes. The samples were equilibrated on a nutating mixer for 1 h at room temperature. After equilibration, both the reaction and control samples were centrifuged at 3,500 RPM for 5 min, and the supernatants were decanted and stored for further analysis using ICP-OES.

2.8 ICP-OES Parameters:

ICP-OES analysis was performed using a Perkin Elmer Optima 8300 ICP-OES (Perkin Elmer, Shelton CT) with Winlab32 software. The parameters used for the analysis are shown in Table 1. If samples were found to be outside of the calibration range of the ICP-OES, then the samples were diluted to fall within the calibration range for the instrument. Furthermore, only calibration curves that had correlation coefficients (R^2) of 0.99 or better were used to obtain data.

3.0 Results and Discussion:

3.1 X-Ray Diffraction Characterization of the TiS2 nanomaterial:

The diffraction pattern for the synthesized TiS_2 nanomaterial is shown in Figure 1. From the pattern, it was determined that the TiS_2 nanomaterial was in a trigonal geometry and had the P3M1 space group. The refined lattice parameters: a=b=3.397 Å and c=5.747 Å with α=β=90˚

Journal Pre-proof

and γ=120˚. The χ^2 for the fitting was 0.939, which showed an excellent agreement between the fitting and the experimental data [24, 25]. The diffraction peaks located at: 18.17, 35.14, 36.82, 40.17, 52.08, 48.05, 56.55, 63.77, 66.92, and 68.88 in 2 theta represent the: 001, 002, 100, 011, 101, 012, 102, 003, 110, 111, 013, and the 103 diffraction planes of TiS_2, respectively. The diffraction planes were determined using crystallographic data from the literature and the Le Bail fitting procedure in the FullProf software [24-27]. The particle size of the TiS_2 was calculated to be 8.03 ± 0.98 nm using Scherrer's equation. The atomic arrangement of TiS_2 consists of the titanium ions surrounded octahedrally by 6 sulfur atoms, which are linked together to form 2-D sheets. Furthermore, the structure of TiS_2 consists of the stacking of the 2-D layers/ sheets, where each layer stacks on top of another and are held together by van der Waals forces [24].

3.2 SEM analysis

Figure 2 shows the SEM images and EDS collected for the synthesized TiS_2 nanomaterial. Figure 2 A shows a low-resolution SEM image of the synthesized TiS_2. As can be seen Figure 2 A, there is a consistency in the size of the synthesized nanoparticles. The morphology of the synthesized TiS_2 nanoparticles on the other hand is complex, shown in Figure 2 B. Superficially the morphology of the material could be referred to as a "flower". However, the particles are collections of TiS_2 platelets, which gives the appearance of the flower morphology. From the image can also be observed that there are at least two different planes present in the sample, there are edge planes and basal planes. The edge plane occurs at the termination of the basal planes. In the SEM image the edge planes are very small approximately 10 nm whereas the basal planes are large 100's of nm across. This trend was also observed in the XRD, the 18.25° (in 2 theta) or the 001 plane represents the stacking plane or the edge planes

Journal Pre-proof

of TiS_2. From the diffraction pattern the 001 plane is broad with low intensity, indicating very low stacking or small number of edge planes. Whereas the diffraction peak at 40.04° (in 2 theta) or the 011 and 101 planes have a diffraction peak that is much higher in intensity and smaller FWHM. The higher intensity and shaper peak indicate a much larger plane in the crystal. The data indicates that the basal plane in the crystal is much larger than the edge planes (or stacking). Figure 2 C shows the EDS spectrum collected from the sample, which indicates the presence of carbon, oxygen, sulfur, chlorine, and titanium. The presence of carbon, oxygen, and chlorine in low amounts in the sample are not surprising, due to the synthesis conditions: a solvothermal reaction using titanium(IV) chloride elemental sulfur, and a high boiling point carbon based solvent. The presence of the oxygen in the sample may be due to the washing procedure and adsorption of oxygen onto the surface of the TiS_2.

3.3 pH Batch Study:

The binding of Cu^{2+} and Pb^{2+} onto the TiS_2 nanomaterial from pH 2 to pH 6 is presented in Figure 3. As can be seen in Figure 3, the sorption of Cu^{2+} at pH 2 was approximately 100% and decreases to 55% binding at pH 3. There was a significant decrease in the binding of Cu^{2+} onto TiS_2 nanoparticles moving from pH 2 to pH 3. In general, as the pH increased, the binding of Cu^{2+} ions was observed to decreased continually to approximately 10% binding observed at pH 6. A similar trend was observed for the sorption of Pb^{2+} ions onto the TiS_2 nanomaterial. The binding was observed to be approximately 100% at pH 2 and decrease steadily to approximately 60% binding at pH 6. pH 2 was chosen as the optimal binding pH for adsorption due to the highest removal of both metal ions was observed at this pH. The binding results of the present study show an opposite trend compared to many of the results in the literature with other

Journal Pre-proof

materials [1,5, 15-16, 29, 30]. For instance, the sorption of Cu^{2+} onto graphene oxide increased as the initial pH of the solution increased from pH 1 to pH 7 [5]. The binding of Cu^{2+} and Pb^{2+} using pristine biochar started below 20% binding at pH 2 and increased to approximately 90% binding at pH 7, whereas engineered biochar reached 100% removal for both Cu^{2+} and Pb^{2+} ions at pH 7 [19]. Several other materials have also shown increasing binding with increasing pH, such as: zero valent iron particles, CuO, meranti wood, and graphene oxide nanomaterials [3,5,15-16,18,20]. The removal of Cu^{2+} and Pb^{2+} was studied using CuO, Fe_3O_4, and ZnO nanomaterials by Mahdavi *et al.*[18]. The results from Mahdavi *et al.,* showed the binding of both Cu^{2+} and Pb^{2+} with Fe_3O_4 and CuO increased with increasing pH, whereas the binding of both ions with ZnO was observed to be pH independent and remained constant throughout the study [18]. In a separate study, also by Mahdavi *et al.* showed an increase in the binding of Cu^{2+} and Pb^{2+} to TiO_2 and Al_2O_3 nano-adsorbents as the pH of the solution was increased [31]. However, the sorption of both Cu^{2+} and Pb^{2+} ions with MgO was not affected when the pH was varied between pH 2 and 7 [31]. Similarly, the sorption of Cu^{2+} to Fe_7S_8 was observed to be pH independent with 100% binding occurring from pH 2 to 6, whereas the binding of Pb^{2+} was observed to increase as the pH of the solution increased [32]. Tamez *et al.,* showed an increasing binding trend for the sorption of Cu^{2+} and Pb^{2+} with Fe_3O_4 as the pH increased from pH 2 to 6 [1]. Similarly, the sorption of Cu^{2+} with Fe_2O_3 showed an increase in binding from pH 2 to 6; however, the binding of Pb^{2+} with the same nanomaterial showed an initial increase from pH2 through 4 and decreased in binding as pH increased to pH 6 [1]. As mentioned earlier, the binding of both the Cu^{2+} and Pb^{2+} to the TiS_2 nanomaterial followed an opposite binding trend decreasing with increasing pH. There are several common factors involved in the binding/sorption of metal ions to adsorbents, such as surface charge, ion charge, the availability

Journal Pre-proof

of binding sites, which can be related to dissociation constants. Also, the ion affinity and ability to form bonds with surface groups plays a crucial role in adsorption. Within the present study the ability of Cu^{2+} and Pb^{2+} to form metal-sulfur bonds may control the binding of these ions to the TiS_2 nanomaterial. Both CuS and PbS are generally formed under acidic conditions as is shown in the literature [32,33]. Low pH for Cu^{2+} and Pb^{2+}, sulfur bond formation could translate to higher binding or removal under acidic conditions. The observed higher binding in the presence study may be indicating that the interaction between the Cu^{2+} and Pb^{2+} ions with the TiS_2 is the formation of a chemical bond not just through physical sorption.

3.4 Capacitance and Thermodynamics Study:

The results for the sorption/ isotherm studies for Cu^{2+} and Pb^{2+} binding to the TiS_2 nanomaterial after a 1 hr contact time at 4˚C, 22˚C, and 45˚C are shown in Figure 4. The binding for both ions was determined to follow the Langmuir isotherm model. The linearized Langmuir isotherms are shown in Figure 4, with the associated linear fitting. Figure 4 A shows the binding of the Pb^{2+} ions to the TiS_2 nanomaterial and Figure 4B shows the Cu^{2+} binding to the TiS_2 nanomaterial. In addition, the correlation coefficients (R^2) for the fittings are also shown in Figure 4, which were for the most part are 0.99 or better. The exception being the 20°C isotherm for the binding of the Pb^{2+} to the TiS_2 nanomaterial. The Langmuir isotherm was determined to be the isotherm based on the goodness of fit between the model and the data. The Langmuir isotherm defined for the adsorption of a monolayer and linear form of the model is shown below in Eq. (1):

$$\frac{1}{q_e} = \frac{1}{q_m} + \frac{1}{K_a q_m C_e} \qquad (1)$$

Journal Pre-proof

Where q_e is the amount of sorbate bound to the sorbent (mg/g), q_m is the maximum binding capacity (mg/g), K_a is a constant, C_e is the equilibrium concentration of the solution.

As can be seen in Table 2, the capacity of the nanomaterial for the sorption of Cu^{2+} starts at 244 mg/g (3.84 mmol/g) at 4˚C and decreases with an increasing temperature. At 45˚C, the sorption for Cu^{2+} was at 154 mg/g (2.42 mmol/g). On the other hand, the capacity for Pb^{2+} at 4˚C was 32 mg/g (0.16 mmol/g) and was observed to increase to 357 mg/g (1.72 mmol/g) at 45˚C. The decrease in capacity of the TiS_2 for Cu^{2+} as the temperature increased, is indicative of an exothermic reaction occurring whereas the increase in capacity for Pb^{2+} indicates an endothermic process for the binding.

The adsorption capacities observed for the binding of Cu^{2+} and Pb^{2+} with other nano-adsorbents are presented in Table 3. For example, Fe-water treated residues have shown binding capacities of 6 mg/g and 22 mg/g for Cu^{2+} and Pb^{2+}, respectively [34]. Additionally, graphene oxide has proved to have high sorption capacities of 530, 345, 294, and 1119 mg/g for Cd^{2+}, Zn^{2+}, Cu^{2+}, and Pb^{2+}, respectively [16]. Red mud and activated carbon from pinecones have exhibited similar binding trends [35,36]. Mahdavi et al., showed that TiO_2 had binding capacities of 50.2 mg/g and 21.7 mg/g for the sorption of Cu^{2+} and Pb^{2+} [31]. Except for graphene oxide, the binding capacity of TiS_2 for Cu^{2+} and Pb^{2+} ions are comparable to the literature values. In fact, in many cases, the binding capacity of TiS_2 for Cu^{2+} and Pb^{2+} ions to are higher than the literature values for other materials. The higher binding capacities indicate a stronger interaction between Cu^{2+} and Pb^{2+} ions and the TiS_2.

The thermodynamics study was performed in conjunction with the binding capacity study, the data from the isotherm studies was used for the determination of the thermodynamics of the binding process. From the isotherm data performed at different temperatures the Gibbs

Journal Pre-proof

free energy, enthalpy, and entropy can be determined and are shown in Table 4. The relationships between thermodynamic parameters and the adsorption isotherms are shown below in Eqs. (2) and (3).

$$\Delta G = -RT(Lnk_d) \quad (2)$$

$$Ln(k_d) = \frac{\Delta S}{R} - \frac{\Delta H}{RT} \quad (3)$$

Where ΔG is the change in Gibbs free energy, R is the gas constant (8.314 J mol^{-1} K^{-1}), T is the temperature in Kelvin, K_d is the distribution coefficient, ΔH is the change in enthalpy, and ΔS is the change in entropy. ΔG was determined for both Cu^{2+} and Pb^{2+} at all three temperatures, using eq 2. Whereas ΔH and ΔS were determined graphically by plotting Ln K_d vs 1/T (in K). A plot of Ln K_d vs 1/T (in K) has a slope that is related to ΔH and an intercept, which is related to ΔS. The thermodynamic plots for the binding data that shown in Figure 5. In addition, the thermodynamic parameters for the sorption process for both ions are presented in Table 4. According to the results, ΔG for the sorption of Cu^{2+} with TiS_2 ranged from -0.003 kJ/mol to 2.00 kJ/mol from 4˚C to 45˚C. The data indicates that the reaction was near equilibrium at 4˚C and becomes non-spontaneous at higher temperatures. Whereas ΔG for the sorption of Pb^{2+} onto the TiS_2 was observed to range from -2.55 kJ/mol to -16.33 kJ/mol from 4˚C to 45˚C, which indicates that the sorption process becomes more spontaneous as the temperature increases. In a previous study conducted by Rafiq et al., the sorption of Cu^{2+} with MgO was spontaneous and near equilibrium with temperature ranges from 323-343 K with ΔG values from -0.35 to -3.26 kJ/mol [37]. Similarly, the sorption of Cu^{2+} with ZnO was spontaneous at the same temperatures

Journal Pre-proof

with ΔG values of -94.43 to -95.37 kJ//mol, respectively [37]. Additionally, Ben-Ali *et al.,* showed that the sorption of Cu^{2+} with pomegranate peel at high temperatures was spontaneous with ΔG values of -5.358 kJ/mol and -7.409 kJ/mol at 303 K and 313 K, respectively [38]. Kumar *et al.,* showed that ΔG for the binding of Pb^{2+} with ZnO nanorods was -8.41, -9.42, and -10.07 kJ/mol at 303 K, 313 K, and 323 K respectively [39]. Furthermore, in a study conducted by Sonmezay *et al.,* ΔG for the sorption of Cu^{2+} with manganese oxide minerals was -27.69, -28.81, and -29.84 kJ/mol at 298, 308, and 318 K, respectively [40]. Zou *et al.,* showed that ΔG for the binding of both Cu^{2+} and Pb^{2+} onto manganese oxide coated zeolite was -50.5, -53.5, and -56.5 kJ/mol and -50.5, -53.6, and -56.7 kJ/mol, respectively at 288, 303, and 313 K [41]. Zepeda *et al.,* showed that the reaction between Cu^{2+} and SnO_2 was non-spontaneous at low temperatures and spontaneous at high temperatures with ΔG values ranging from 3.13 kJ/mol to -0.86 kJ/mol with temperatures ranging from 4˚C to 45˚C, respectively [42]. The data presented in the current study are within range and are comparable to the data presented in similar studies [37-42]. However, the opposing trend in the binding of the Cu^{2+} ion and Pb^{2+} ions observed with the TiS_2 material has not been observed in many studies. As previously mentioned, the Cu^{2+} ion decreases in binding with increasing temperature, this indicates an exothermic process involved in the binding. Whereas the binding of the Pb^{2+} ions increased with increasing temperature to the TiS_2 indicates an endothermic binding process was occurring. The explanation for these opposing binding processes can explained from the thermodynamic data for compound (for PbS and CuS) formation. The $\Delta G°_f$'s for both the copper and Pb sulfides are -53.6 kJ/mol and -98.7 kJ/mol, respectively [43]. The thermodynamic data for the formation of CuS and PbS, indicates the PbS reaction is more favorable than CuS. The more favorable formation of the PbS is indicated by the much larger negative value of $\Delta G°_f$ observed for PbS compared with the $\Delta G°_f$

Journal Pre-proof

for CuS. Furthermore, the entropy of formation for PbS (91.2 J/molK) is also larger than the entropy of formation for CuS (66.5 J/molK). Given the combination of processes involved in the binding of both Cu^{2+} and Pb^{2+}, along with the favorable formation of the PbS over CuS, it is not surprising that the thermodynamics of binding is more favorable with Pb^{2+} to TiS_2 than Cu^{2+} to TiS_2. The thermodynamics of compound formation for the PbS and CuS are exemplified in the diffraction patterns shown in Figure 6. The diffraction pattern for the reaction between the Cu^{2+} and the TiS_2 (Figure 6 A), which shows no change in the diffraction pattern from that observed for pure TiS_2 (shown in Figure 1). However, the Pb^{2+} ion reaction with the TiS_2 nanomaterial shows the development of new diffraction peaks in the pattern. The new diffraction peaks shown in Figure 6 B are the diffraction peaks for galena or PbS, this indicates the formation of PbS after reaction [28]. The new diffraction peaks correspond to the PbS 111 (30.51°), an increase in the sized of the diffraction peak at 35.37°, when compared to TiS_2 diffraction pattern (the PbS 200 shows at this angle), the PbS 220 (50.89°), and PbS 311 (60.55°). The fitting of the copper binding to the TiS_2 material had a reduced χ^2 of 1.72, and the fitting of the TiS_2 reacted with the PbS has a χ^2 of 3.56. Both these fitting show good agreement between the data and the fitting.

As previously mentioned, ΔS and ΔH were calculated by plotting LnK_d against 1/T (in K) as shown in Figure 6. ΔH was determined from the slope of the line whereas ΔS was calculated using the intercept of the plot. According to the results shown in Table 4, ΔH for the binding of Cu^{2+} was -14.24 kJ/mol indicating an exothermic process occurring during the sorption of Cu^{2+} with TiS_2. On the other hand, the value of ΔH for the sorption of Pb^{2+} was 95.8 kJ/mol indicating that an endothermic process occurs for Pb^{2+} binding to the TiS_2. Zepeda et al., showed a ΔH of 28.73 kJ/mol for sorption of Cu^{2+} with SnO_2 nanoparticles indicating an endothermic reaction [42]. Similarly, in a previous study by Cantu *et al.*, showed that the reactions of Cu^{2+} and Pb^{2+}

Journal Pre-proof

with Fe_7S_8 were endothermic with ΔH values of 153.51 kJ/mol and 55.81 kJ/mol, respectively [23]. In addition, the magnitude of ΔH, the binding for Cu^{2+} indicates that a reaction occurs thorough ion exchange whereas Pb^{2+} binding occurs via chemisorption. According to the literature, the sorption processes with ΔH ranging from 8.0 to 16.0 kJ/mol correspond to ion exchange whereas ΔH values greater than 40 kJ/mol are attributed to chemisorption which supports the formation of a PbS compound after sorption, [44]. For chemisorption, the formation of a chemical bond occurs between the adsorbate and adsorbent, which is shown in Figure 6 B the formation of the PbS after reaction between Pb^{2+} with the TiS_2.

3.5 Kinetics Study:

The results for the kinetics study for the sorption of Cu^{2+} and Pb^{2+} to TiS_2 nanomaterial are shown in Figure 7. Figure 7A shows the kinetics for the binding of Cu^{2+} ions to the TiS_2 nanomaterial. Whereas Figure 7 B shows the kinetics for the binding of the Pb^{2+} ions to the TiS_2 nanomaterial. The respective equations for the curve fittings and correlation coefficients for each curve fitting are also provided in Figure 7. As shown in Figure 7, the sorption of Cu^{2+} and Pb^{2+} with the TiS_2 nanoparticles was found to follow a zeroth order kinetics model, all the correlation coefficients, R^2, were observed to range from 0.98 to 1.0. The zeroth order reaction was chosen due to plotting of the concentration against time gave a straight line. A zeroth order kinetics model indicates that the sorption of each of the metal ions is dependent on the contact time with the TiS_2 nanoparticles. The zeroth order reaction model equation is given in Eq. (4).

$$[C] = k[t] \qquad (4)$$

Where C is the concentration of the ions at any given time, t, is the adsorption time in minutes, and k is the rate constant for the metal-ion adsorption onto the nano-sorbent at equilibrium. The zeroth order kinetic model has been found to fit with many adsorption studies [31, 42, 45, 46].

Journal Pre-proof

While other studies investigating the sorption of Cu^{2+} and Pb^{2+} with nanomaterials have shown a pseudo-second order kinetics model can also be suitable [15-16, 18, 41, 47].

From the kinetics data the activation energies for the binding of both Cu^{2+} and Pb^{2+} ions were determined. By performing the kinetics studies at three different temperatures. The activation energy was determined using Arrhenius equation given in eq. (5).

$$Ln(k) = -\frac{E_a}{RT} - Ln(A) \quad (5)$$

Where Ln(k) is the natural log of the rate constant; E_a is the activation energy; R is the gas constant (8.314 J/mol K); T is the temperature in Kelvin; Ln(A) is the frequency factor for the reaction. The Arrhenius plot was constructed by plotting Ln(k) vs 1/T in Kelvin and is shown in Figure 8. From the Arrhenius the slope of the line in the plot is equal to –Ea/R. The study shows activation energies of 19.7 and 54.1 kJ/mol for the binding of Cu^{2+} and Pb^{2+}, respectively as shown in Table 5. Studies have shown that the type of adsorption can be identified based on the magnitude of the activation energy, where energies below 20 kJ/mol are indicative of physisorption [48-50]. Sorption reactions with activation energies found to range from 20 to 80 kJ/mol are indicative of chemisorption [48-50]. Based on the results, the sorption for Pb^{2+} ions occur through chemisorption since the activation energies are clearly above 20 kJ/mol [48-50]. Whereas the binding of the Cu^{2+} ions occurs through a combination of both physisorption and chemisorption process, the activation energy for the binding was close to 20 kJ/mol. These different adsorption mechanisms could be related to the less thermodynamically favorable formation of the Cu-S bonds as mentioned earlier and shown in Figure 6.

3.6 Interference Study:

Journal Pre-proof

Figure 9 A, B, and C show the results for the individual interference and combination interferences studies for the sorption of Cu^{2+} and Pb^{2+} to the TiS_2 nanomaterial. Common hard cations found in natural water systems (Na^+, K^+, Ca^{2+}, and Mg^{2+}) were used as possible interference ions for the sorption of both Cu^{2+} and Pb^{2+} to the TiS_2 nanomaterial. The sorption results of Cu^{2+} in the presence of Na^+ (Figure 9 A) showed no effect at low concentrations and remained constant at 100% binding. However, in the presence of 1000 ppm Na^+, the binding was observed to decrease to approximately 50%. A similar trend was observed in the presence of K^+ and Ca^{2+} in which the binding decreased to 60% in the presence of 1000 ppm K^+ and 60% binding with 300 ppm Ca^{2+}. Mg^{2+} ions on the other hand, show no effect at low concertation but at intermediate and high concentrations, the binding of the Cu^{2+} ions were observed to decrease with increasing concentrations above 3 ppm. At high concentrations, the presence 1000 ppm of Mg^{2+} decreased the Cu^{2+} binding from 100% to 45%. In a study conducted by Tamez *et al.*, the presence of the combined interferences, showed no interference in the binding of Cu^{2+} with Fe_3O_4 nanomaterial [1]. However, in the same study, the presence of Mg^{2+} caused an antagonistic effect on the binding of Cu^{2+} with Fe_2O_3 nanomaterial as the concentration of the Mg^{2+} increased [1]. A study by Cantu *et al.*, showed that the increase in concentration of the interfering cations resulted in an antagonistic effect on the binding of Cu^{2+} with Fe_7S_8.

As seen in Figure 9 B, the presence of any of the cation interferences had a little or no effect on the binding of Pb^{2+} to the TiS_2 nanomaterial. Even in the presence of increasing interference concentrations up to 1000 ppm no decrease in binding was observed for Pb^{2+}. Tamez *et al.*, also observed a similar trend with the binding of Pb^{2+} in the presence of Na^+, K^+, Mg^{2+}, or Ca^{2+} with an Fe_3O_4 adsorbent [1]. The presence of Na^+ or Ca^{2+} was observed to have a synergistic effect on the sorption of Pb^{2+} with Fe_2O_3. An increase in Na^+ or Ca^{2+} concentration

Journal Pre-proof

was observed to cause an increase in the sorption of Pb^{2+} [1]. Similarly, the results by Cantu *et al.,* showed that for the sorption of Pb^{2+} onto Fe_7S_8, little to no effect in the ion binding was observed as the concentration of the cations were increased [31].

The results of the combined interference study are shown in Figure 9 C. As can be seen in Figure 9 C, the Cu^{2+} binding low and appeared to be concentration independent. The binding of Cu^{2+} in the combined interference study shown erratic behavior with no observable trend. The Cu^{2+} ions were observed to bind from approximately 30% to up to a maximum of approximately 60%. However, the binding of Lead was unaffected in the presence of the hard cations ions. The Pb^{2+} binding was maintained at approximately 100% even in the presence of 1000 ppm of combined interference concentration (the solution contained 1000 ppm of each interferences Na, K, Ca, and Mg). The combined interference data indicates that there is some preferential binding for both Cu^{2+} ion and Pb^{2+} ions to the TiS_2 nanomaterial, which would indicate chemisorption is involved in the binding process for both ions. The preferred binding is indicated by the binding data at 300 ppb of either Cu^{2+} or Pb^{2+} and 4000 ppm total ion concentration the heavy metals bound to the nanomaterial. The solutions have Pb^{2+} and Cu^{2+} molar ratio to interfering ions of 1: 2035 and 1:6635, respectively. At such a high molar ratio interference to Pb^{2+} and Cu^{2+} the metal ion binding should be eliminated. However, the selectivity in the binding comes from the determined binding mechanism chemisorption for Pb^{2+} and a combination of physisorption and chemisorption for Cu^{2+} ions. Physisorption or ion exchange mechanisms would be overcome by the high concentrations of hard cations and the binding of the Pb^{2+} and Cu^{2+} would be eliminated.

4.0 Conclusions

Journal Pre-proof

The sorption of both Cu^{2+} and Pb^{2+} with the TiS_2 nanomaterial was determined to be pH dependent, with both ions binding high at low pH and decreasing with increasing pH. The adsorption capacity for Cu^{2+} was observed to decrease as the temperature increased indicating an exothermic reaction, whereas Pb^{2+} binding capacity was observed to increase as the reaction temperature increased indicating an endothermic reaction. The thermodynamic data in the present study showed the sorption of Cu^{2+} with TiS_2 was non-spontaneous and exothermic. However, the Pb^{2+} binding to the TiS_2 was spontaneous at all temperatures studied and was an endothermic process. The kinetics data for the sorption of both Cu^{2+} and Pb^{2+} were determined to follow a zeroth order kinetic model, which indicates a direct relationship between the reaction concentration and contact time. In addition, the data indicates the binding occurs through a combination of chemisorption and physisorption for Cu^{2+} binding. Pb^{2+} was determined to bind through chemisorption only. High concentrations of the hard cation interfering species were only observed to decrease the binding of Cu^{2+} and had no effect on the Pb^{2+} binding.

Acknowledgments

Authors would like to thank the NIH UTPA RISE program (Grant Number 1R25GM100866-03). The Department of Chemistry at the University of Texas Rio Grande Valley is grateful for the generous support provided by a Departmental Grant from the Robert A. Welch Foundation (Grant No. BX-0048). M. Alcoutlabi would like to acknowledge the support from NSF PREM /award/ under grant No. DMR-1523577: UTRGV-UMN Partnership for Fostering Innovation by Bridging Excellence in Research and Student Success.

Journal Pre-proof

References:

1. C. Tamez, R. Hernandez, J.G. Parsons, Removal of Cu (II) and Pb (II) from Aqueous solution using engineered iron oxide nanoparticles, Microchem. J. 125 (2016) 97-104.

2. Y. Liu, L. Chen, Y. Li, P. Wang, Y. Dong, Synthesis of magnetic polyaniline/graphene oxide composites and their applications in the efficient removal of Cu(II) from aqueous solutions, J. Environ. Chem. Eng. 4 (2016) 825-834.

3. A. Ahmad, M. Rafatullah, O. Sulaiman, M.H. Ibrahim, Y.Y Chi, B.M. Siddique, Removal of Cu(II) and Pb(II) ions from aqueous Solutions by adsorption on sawdust of meranti wood, Desalination 247 (2009) 636-636.

4. L.M. Gaetke, C.K. Chow, Copper toxicity, oxidative stress, and antioxidant nutrients, Toxicol. 189 (2003) 147-163.

5. W. Wu, Y. Yang, H. Zhou, T. Ye, Z. Huang, R. Liu, Y. Kuang, Highly efficient removal of Cu(II) from aqueous solution by using graphene oxide, Water Air Soil Pollut. 224 (2013) 1372.

6. P.G. Georgopoulos, S.W. Wang, I.G. Georgopoulos, M.J. Yonone-lioy, P.J. Lioy, Assessment of human exposure to copper: a case study using the NHEXAS database, J.f Exposure Sci. Environ. Epidemiol. 16 (2006) 397-409.

7. E. Mosayebi, S. Azizian, Study of copper ion adsorption from aqueous solution with different nanostructured and microstructured zinc oxides and zinc hydroxide loaded on activated carbon cloth, J. Mol. Liq. 214 (2016) 384-389.

8. H. Needleman, Lead Poisoning, Ann. Rev. Med. 55 (2004) 209-222.

9. Ab Latif Wani, Anjum Ara, and Jawed Ahmad Usmani. Lead toxicity: a review Interdiscip Toxicol. 2015 Jun; 8(2): 55–64.

10. Nikolas C Papanikolaou, Eleftheria G Hatzidaki, Stamatis Belivanis, George N Tzanakakis, Aristidis M Tsatsakis. Lead toxicity update. A brief review. Med. Sci. Monit. 11 (2005) RA 329-336

11. E. Eren, B. Afsin, Y. Onal, Removal of lead ions by acid activated and manganese oxide-coated bentonite, J. Hazard. Mater. 161 (2009) 677-685.

12. F. Fu, Q. Wang, Removal of heavy metal ions from wastewaters: A review, J. Environ. Manage. 92 (2011) 407-418.

13. A.N. Anthemidis, K.G. Ioannou, Recent developments in homogeneous and dispersive liquid-liquid extraction for inorganic elements determination. A review, Talanta 80 (2009) 413-421/

Journal Pre-proof

14. A. Azimi, A. Azari, M.Rezakazemi, M. Ansarpour, Removal of Heavy Metals from Industrial Wastewaters: A Review, ChemBioEng Rev 4 (2017) 37–59.

15. A.A. Farghali, M. Bahgat, A. Enaiet Allah, M.H. Khedr, Adsorption of Pb(II) ions from aqueous solutions using copper oxide nanostructures, BENI-SUEF Univ. J. Basic Appl. Sci. 2 (2013) 61-71.

16. R. Sitko, E. Turek, B.Zawisza, E. Malicka, E. Talik, J. Heimann, A. Gagor, B. Feist, R. Wrzalik, Adsorption of divalent metal ions from aqueous solutions using graphene oxide. Dalton Trans. 42 (2013) 5682-5689.

17. X. Wang, Z. Chen, S. Yang, Applications of graphene oxides for the removal of Pb(II) ions from aqueous solutions: Experimental and DFT calculation. J. Mol. Liq. 211 (2015) 957-964.

18. S. Mahdavi, M. Jalali, A. Afkhuami, Removal of heavy metals from aqueous solutions using Fe3O4, ZnO, and CuO nanoparticles, Journal of Nanoparticle Research 14 (2012) 846.

19. H. Wang, B. Gao, S. Wang, J. Fang, Y. Xue, K. Yang, Removal of Pb(II), Cu(II), and Cd(II) from aqueous solutions by biochar derived from $KMnO_4$ treated wood, Biosour. Technol. 197 (2015) 356-362.

20. A.M. Azzam, S.T. El-Wakeel, B.B. Mostafa, M.F. El-Shahat, Removal of Pb, Cu, and Ni from aqueous solution using nano scale zero valent iron particles, J. Environ. Chem. Eng. 4 (2016) 2196-2206.

21. M. Fouladgar, M. Beheshti, H. Sabzyan, Single and binary adsorption of nickel and copper from aqueous solutions by γ-alumina nanoparticles: Equilibrium and kinetic modeling, J. Mol. Liq. 211 (2015) 1060-1073.

22. K.E. Engates, H.J. Shipley, Adsorption of Pb, Cd, Cu, and Zn to titanium dioxide nanoparticles: effect of particle size, solid concentration, and exhaustion, Environ. Sci. Pollut. Res. 18 (2011) 386-395.

23. J. Cantu, D.F. Gonzalez, Y. Cantu, T.M. Eubanks, J.G. Parsons, Thermodynamic and kinetic study of the removal of Cu^{2+} and Pb^{2+} ions from aqueous solution using Fe_7S_8 nanomaterial, Microchem. J. 140 (2018) 80–86.

24. R.R. Chianelli, J.C. Scanlon, A.H. Thompson, Structure refinement of stoichiometric TiS_2, Mater. Res. Bull, 10 (1975) 1379-1382.

25. S. Prakabar, C.W. Bumby, R.D. Tilley, Liquid-phase synthesis of flower-like and flake-like titanium disulfide nanostructures, Chem. Mater. 21 (2009) 1725-1730.

Journal Pre-proof

26. Rodriguez-Carvajal J. Recent advances in magnetic structure determination by neutron powder diffraction. Physica B. 1993;192:55–69.

27. LeBail A, Duroy H, Fourquet JL. Ab-Initio Structure Determination of LiSbWO8 By X-Ray Powder Diffraction. Mat. Res. Bull. 1988;23:447–452.

28. Y. Noda, K. Matsumoto, S.Ohba, Y. Saito, K. Toriumi, Y. Iwata, I. Shibuya. Temperature Dependence of Atomic Thermal Parameters of Lead Chalcogenides, PbS, PbSe and PbTe. Acta Crystallographica C43 (1987), 1443-1445.

29. Q. Fan, Z. Li, H.Z. Jia, J. Xu, W. Wu, Adsorption of Pb(II) on palygorskite from aqueous solution: Effects of pH, ionic strength and temperature. Appl Clay Sci. 45 (2009) 111-116.

30. R.R. Gadde, H.A. Laitinen, Studies of heavy metal adsorption by hydrous iron and manganese oxides, Anal. Chem. 46, 13 (1974) 2022-2026.

31. S. Mahdavi, M. Jalali, A. Afkuami, Heavy metal removal from aqueous solutions using TiO_2, MgO, and Al_2O_3, Chem. Eng. Comm. 200 (2013) 448–470.

32. S I Sadovnikov, A I Gusev. Chemical deposition of nanocrystalline lead sulfide powders with controllable particle size J. Alloys Compd. 586 105 (2014)

33. J.-Y. Gong, S.-H. Yu, H.-S. Qian, L.-B. Luo, and X.-M. Liu. Acetic Acid-Assisted Solution Process for Growth of Complex Copper Sulfide Microtubes Constructed by Hexagonal Nanoflakes Chem. Mater. 2006, 18, 2012-2015

34. P. Castaldi, M. Silvetti, G. Garau, D. Demurtas, S. Deiana, Copper(II) and lead(II) removal from aqueous solution by water treatment residues, J. Hazard. Mater. 283 (2015) 140-147.

35. H. Nadaroglu, E. Kalkan, N. Demir, Removal of copper from aqueous solution using red mud, Desalination 251 (2010) 90-95.

36. M. Momcilovic, M. Purenovic, A. Bojic, A. Zarubica, M. Randelovic, Removal of lead(II) ions from aqueous solutions by adsorption onto pine cone activated carbon, Desalination 276 (2011) 53-59.

37. Z. Rafiq, R. Nazir, Durr-e-Shahwar, M.R. Shah, S. Ali, Utilization of magnesium and zinc oxide nano-adsorbents as potential materials for treatment of copper electroplating industry wastewater, J. Environ. Chem. Eng. 2 (2014) 642-651.

38. S. Ben-Ali, I. Jaouali, S. Souissi-Najar, A. Ouederni, Characterization and adsorption of raw pomegranate peel biosorbent for copper removal, J. Cleaner Prod. 142 (2017) 3809-3821.

Journal Pre-proof

39. K.Y. Kumar, H.B. Muralidhara, Y.A. Nayaka, J. Balasubramanyam, H. Hanumanthappa, Hierarchically assembled mesoporous ZnO nanorods for the removal of lead and cadmium by using differential pulse anodic stripping voltammetric method. Power Technology 239 (2013) 208-216.

40. A. Sonmezay, M.S. Oncel, N. Bektas, Adsorption of Lead and Cadmium Ions from Aqueous solutions using manganoxide minerals, Trans. Nonferrous Met. Soc. China. 22 (2012) 3131-3139.

41. W. Zou, R. Han, Z. Chen, Z. Jinghua, J. Shi, Kinetic study of Cu(II) and Pb(II) from aqueous solutions using manganese oxide coated zeolite in batch mode, Colloids Surf., A. 279 (2006) 238-246.

42. A.M. Zepeda, D. Gonzalez, L. Gonzalez Heredia, K. Marquez, C. Perez, E. Pena, K. Flores, C. Valdes, T.M. Eubanks, J.G. Parsons, J. Cantu, Removal of Cu^{2+} and Ni^{2+} from aqueous solution using SnO_2 nanomaterial effect of: pH, time, temperature, interfering cations, Microchem. J. 141 (2018) 188–196.

43. D. R. Lide Handbook of Chemistry and Physics75th edition. CRC Press, Florida 1994.

44. M.A.Al-Anber,Thermodynamics Approach in the Adsorption of Heavy Metals, Thermodynamics - Interaction Studies - Solids, Liquids and Gases, in: J.C. Moreno Pirajain (Ed.) InTech, 2011 https://doi.org/10.5772/21326

45. S. Luther, N. Brogfeld, J. Kim, J.G. Parsons, Study of the thermodynamics of chromium(III) and chromium(VI) binding to iron(II/III) oxide or magnetite or ferrite and manganese(II) iron (III) oxide or jacobsite or manganese ferrite nanoparticles, J. Colloid Interface Sci. 400((2013) 97–103.

46. N.S. Rajurkar, A.N. Gokarn, K. Dimya, Adsorption of chromium(III), nickel(II), and copper(II) from aqueous solution by activated alumina, Clean–Soil, Air, Water 39 (2011) 767–773.

47. V.K. Gupta, A. Rastogi, Biosorption of lead from aqueous solutions by green algae Spirogyra species: Kinetics and equilibrium studies, J. Hazard. Mater. 152 (2008) 407-414.

48. T. Mahmood, M.T. Saddique, A.Naeem,S. Mustafa, N. Zeb, K.H. Shah, M. Waseem, Kinetic and thermodynamic study of Cd(II), Co(II) and Zn(II) adsorption from aqueous solution by NiO, Chem. Eng. J. 171 (2011) 935–940.

49. H.K. Boparai, M. Joseph, D.M. O'Carroll, Kinetics and thermodynamics of cadmium ion removal by adsorption onto nano zerovalent iron particles, J. Hazard. Mater. 186 (2011) 458–465.

Journal Pre-proof

50. Y. Cantu, A. Remes, A. Reyna, D. Martinez, J. Villarreal, H. Ramos, S. Trevino, C. Tamez, A. Martinez, T. Eubanks, J.G. Parsons, Thermodynamics, kinetics, and activation energy studies of the sorption of chromium(III) and chromium(VI) to a Mn_3O_4 nanomaterial, Chem. Eng. J. 254 (2014) 374–3834.

51. M. Hua, S. Zhang, B. Pan, W. Zhang, L. Lv, Q, Zhang. Heavy metal removal from water/wastewater by nanosized metal oxides: A review, J. Hazard. Mater. 211-212, (2012) 317-331.

52. S.G. Wang, W.X. Gong, X.W. Liu, Y.W. Yao, B.Y Gao, Removal of lead(II) from aqueous solution by adsorption onto manganese oxide-coated carbon nanotubes. Sep. Purif. Technol. 58 (2007) 17-23.

53. Y.H. Chen. F.A. Li, Kinetic study on removal of copper(II) using goethite and hematite nano-photocatalysts, J. Colloid Interface Sci. 347 (2010) 277-281.

54. S. Wang, M. Soudi, L. Li, Z.H. Zhu, Coal ash conversion into effective adsorbents for removal of heavy metals and dyes from wastewater, J. Hazard. Mater. 133 (2006) 243–251.

55. Z. Gao, T.J. Bandosz, Z. Zhao, M. Han, J. Qiu, Investigation of factors affecting adsorption of transition metals on oxidized carbon nanotubes, J. Hazard. Mater. 167 (2009) 357–365.

56. M. Lee, J.H. Park, J.W. Chung, C. Lee, S. Kang, Removal of Pb and Cu ions from aqueous solution by Mn3O4-coated activated carbon, J Ind. Eng. Chem. 21 (2015) 470–475.

Journal Pre-proof

Journal Pre-proof

Figure Legends:

Figure 1: X-ray diffraction pattern for the synthesized TiS_2 nanomaterial.

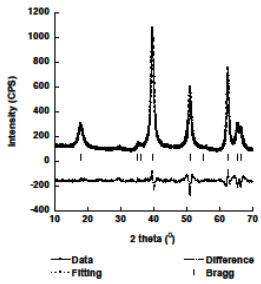

Figure 2: A. SEM image of the synthesized TiS_2 nanomaterial, taken at 1000 x magnification. B. SEM image of the synthesized TiS_2 nanomaterial, taken at 20000 x magnification. C. EDS spectrum recorded for the TiS_2 as synthesized material.

Journal Pre-proof

Journal Pre-proof

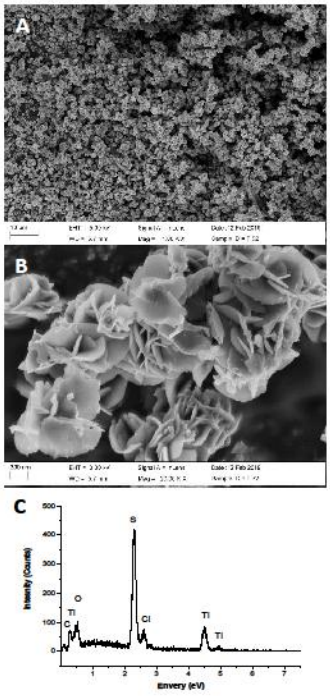

Figure 3: pH profile for the sorption of Cu^{2+} and Pb^{2+} with the TiS_2 nano-sorbent ranging from pH 2 to pH 6.

Journal Pre-proof

Journal Pre-proof

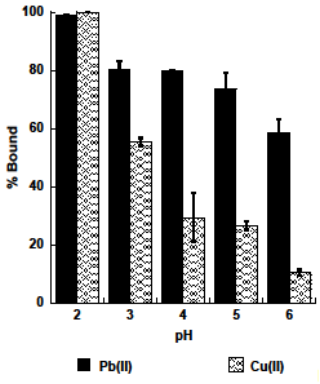

Figure 4: Linearized Langmuir isotherm plots for the binding of Pb^{2+} ions to the TiS_2 nanoparticles at 4℃, 20℃, 45℃ (**A**) and the binding of Cu^{2+} ions to the TiS_2 nanomaterial at 4℃, 20℃, and 45℃(**B**).

Journal Pre-proof

Journal Pre-proof

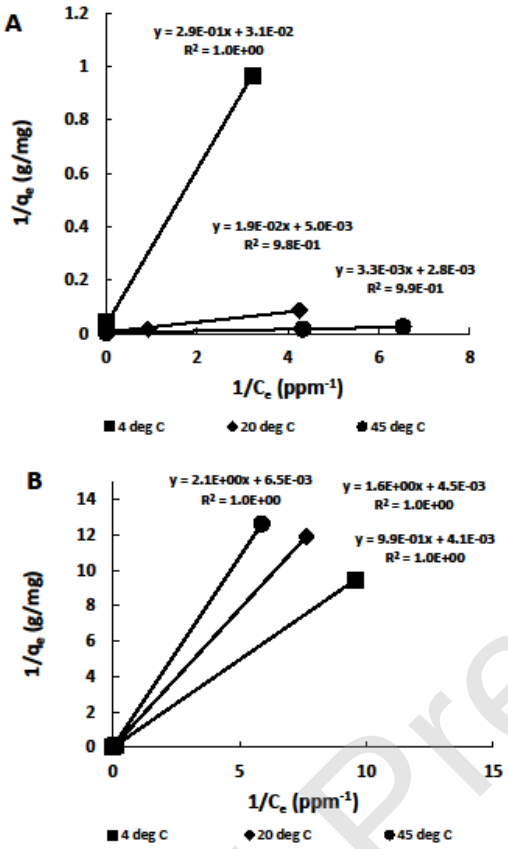

Figure 4

Journal Pre-proof

Journal Pre-proof

Figure 5: Thermodynamic plot for the sorption of Cu^{2+} and Pb^{2+} with the TiS_2 nano-sorbent.

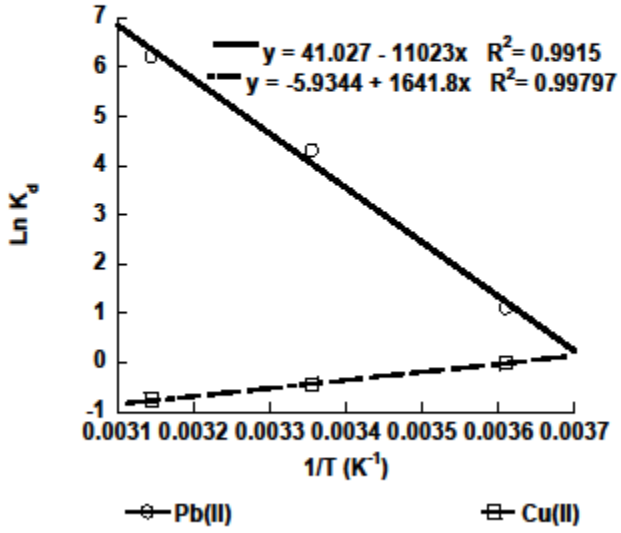

Figure 5

Figure 6: X-ray diffraction pattern of the TiS_2 nanomaterial after reaction with Cu^{2+} ions (A) and Pb^{2+} ions (B).

Journal Pre-proof

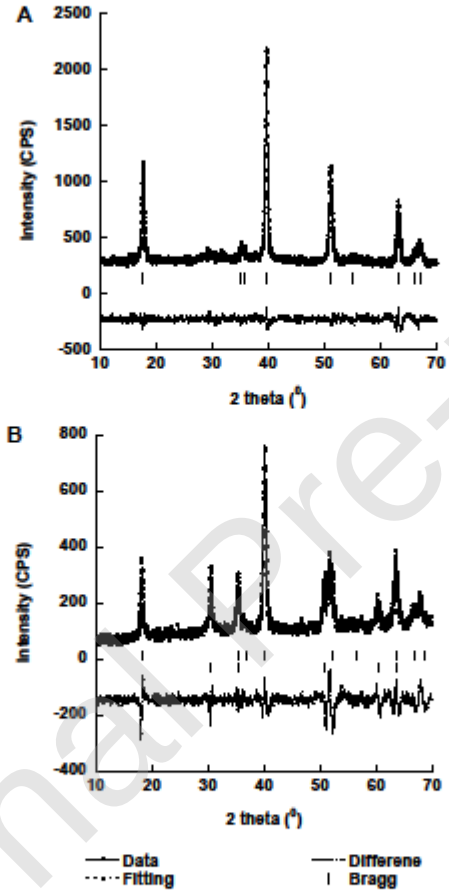

Figure 6

Journal Pre-proof

Journal Pre-proof

Figure 7: Kinetics plots for the reaction for Cu^{2+} (**A**) and Pb^{2+} (**B**) with the synthesized TiS_2 nanomaterial at temperatures of 4. 20, and 45℃

Journal Pre-proof

Journal Pre-proof

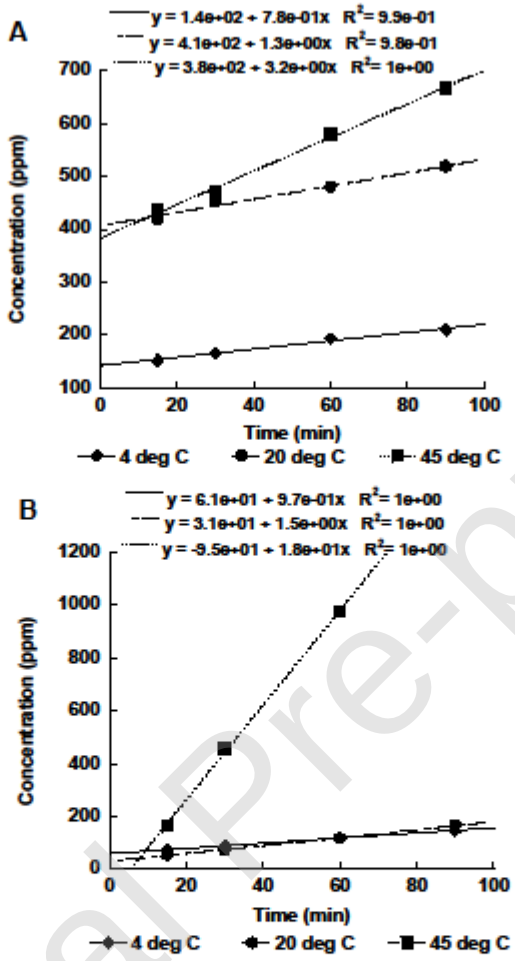

Figure 7

Journal Pre-proof

Journal Pre-proof

Figure 8: Arrhenius plot for the sorption of Cu^{2+} and Pb^{2+} with the TiS_2 nano-sorbent.

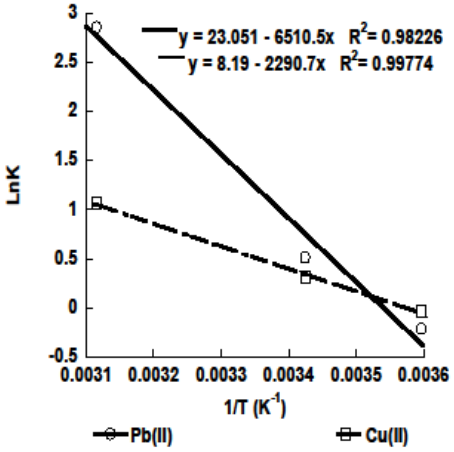

Figure 8

Journal Pre-proof

Journal Pre-proof

Figure 9: A) Sorption of Cu^{2+} to the TiS_2 nano-sorbent with individual cationic interfering species, B) sorption of Pb^{2+} to the TiS_2 nano-sorbent with individual cationic interfering species. C. Sorption of Cu^{2+} and Pb^{2+} to the TiS_2 nano-sorbent in the presence of combined cationic interfering species.

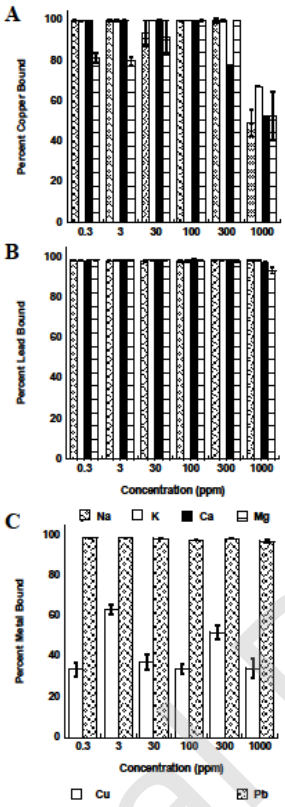

Figure 9

Journal Pre-proof

Journal Pre-proof

Table 1: ICP-OES parameters for the analysis of Cu^{2+} and Pb^{2+} solutions after equilibration with the TiS_2 nanomaterial.

Parameter	**Settings**
λ_{Cu}	327.393 nm
λ_{Pb}	217 nm
RF power	1500 W
Nebulizer	Gemcone (low flow)
Plasma Flow	15 L/min
Auxiliary Flow	0.2 L/min
Nebulizer Flow	0.55 L/min
Sample Flow	1.50 mL/min
Injector	2.0 mm Alumina
Spray Chamber	Cyclonic
Integration Time	20 seconds
Replicates	3

Table 2: Binding capacities for the binding of Cu^{2+} and Pb^{2+} onto the TiS_2 nanomaterial at various temperatures.

Ion	**T (K)**	**Capacity (mg/g)**	**Capacity (mmol/g)**
Pb^{2+}	277 K	32	0.16
	295 K	166	0.80
	318 K	357	1.72
Cu^{2+}	277 K	244	3.83
	295 K	222	3.50
	318 K	154	2.42

Journal Pre-proof

Journal Pre-proof

Table 3: Adsorption capacities for the binding of Cu^{2+} and Pb^{2+} to different nano-adsorbents.

Material	**Ion**	**Capacity (mmol/g)**	**Capacity (mg/g)**	**Reference**
Fe_2O_3	Cu^{2+}	0.23	19.61	[1]
Fe_2O_3	Pb^{2+}	0.31	47.62	[1]
Fe_3O_4	Cu^{2+}	0.81	37.04	[1]
Fe_3O_4	Pb^{2+}	0.58	166.67	[1]
Graphene Oxide	Cu^{2+}	1.84	117.5	[5]
Fe_3O_4	Cu^{2+}	0.49	14.7	[18]
Fe_3O_4	Pb^{2+}	0.23	101.4	[18]
ZnO	Cu^{2+}	0.54	137.5	[18]
ZnO	Pb^{2+}	2.16	112.7	[18]
CuO	Cu^{2+}	0.19	54.1	[18]
CuO	Pb^{2+}	0.85	39.4	[18]
Al_2O_3	Cu^{2+}	0.754	47.9	[31]
Al_2O_3	Pb^{2+}	0.199	41.2	[31]
MgO	Cu^{2+}	2.45	149.1	[31]
MgO	Pb^{2+}	0.717	148.6	[31]
TiO_2	Cu^{2+}	0.79	50.2	[31]
TiO_2	Pb^{2+}	0.105	21.7	[31]
Fe_7S_8	Cu^{2+}	0.102	5.29	[23]
Fe_7S_8	Pb^{2+}	0.039	8.09	[23]
Red mud	Cu^{2+}	0.084	5.35	[35]
SnO_2	Cu^{2+}	0.046	2.95	[42]
CeO_2	Cu^{2+}	0.044	15.4	[51]
CeO_2	Pb^{2+}	0.240	9.2	[51]
MnO_2/CNTs	Pb^{2+}	0.380	78.74	[52]
Fe(OOH) (goethite)	Cu^{2+}	2.350	149.25	[53]
Coal ash	Cu^{2+}	0.661	42.0	[54]
Oxidized carbon nanotubes	Cu^{2+}	0.040	2.57	[55]
Activated Carbon (AC)	Cu^{2+}	0.094	6.09	[56]
Activated Carbon (AC)	Pb^{2+}	0.131	27.17	[56]
Mn_3O_4	Cu^{2+}	0.020	1.24	[56]
Mn_3O_4	Pb^{2+}	0.037	7.57	[56]
Mn_3O_4/AC	Cu^{2+}	0.583	37.04	[56]
Mn_3O_4/AC	Pb^{2+}	0.287	59.52	[56]

Journal Pre-proof

Table 4: Thermodynamic parameters for the sorption of Cu^{2+} and Pb^{2+} with the TiS_2 nanomaterial.

Ion	**ΔG (kJ/mol)**	**ΔH (kJ/mol)**	**ΔS (J/mol)**
Pb^{2+}	-2.55 (277 K) -10.68 (298 K) -16.33 (318 K)	95.8	355.8
Cu^{2+}	-0.003 (277 K) 1.10 (298 K) 2.00 (318 K)	-14.24	-54.1

Table 5: Results for the kinetics study showing the calculated activation energies for the sorption of Cu^{2+} and Pb^{2+} to the TiS_2 nanomaterial.

Ion	**T (K)**	**Ea (kJ/mol)**
Pb^{2+}	277 296 318	54.1
Cu^{2+}	277 296 318	19.7

Journal Pre-proof